Tarnished silver–copper surfaces reduction using remote helium plasma at atmospheric pressure studied by means of high-resolution synchrotron x-ray photoelectron microscopy

Tarnished silver-copper surfaces reduction using remote helium plasma at atmospheric pressure studied by means of high-resolution synchrotron x-ray photoelectron microscopy

Olivier Schalm[a,b], Alessandro Patelli[c], Patrick Storme[a], Amandine Crabbé[d], Stefano Voltolina[e], Vitaliy Feyer[f], Herman Terryn[d]

a: University of Antwerp, Conservation Studies, Blindestraat 9, B-2000 Antwerp, Belgium
b: Antwerp Maritime Academy, Noordkasteel Oost 6, B-2030 Antwerpen, Belgium
c: Padova University, Dept. Physics and Astronomy, Via Marzolo 8, 35131 Padova, Italy
d: Vrije Universiteit Brussel (VUB), Research Group of Electrochemical and Surface Engineering, Pleinlaan 2, B-1050 Brussels, Belgium
e. Veneto Nanotech, Nano Fabrication Facility, Via delle Industrie 9, 30175 Venezia-Marghera, Italy
f. Peter Grünberg Institute (PGI-6) and JARA-FIT, Research Center Jülich, 52425 Jülich, Germany

Highlights

- Top nm layer of tarnished Ag, Ag-Cu alloy and Cu is reduced by afterglow plasma
- The reduction in depth depends on the sulphide compounds in the corrosion layer
- Afterglow plasma reduction mechanism is explained by standard reduction potentials

Abstract
Previous investigations suggested that sulphide layers on pure silver surfaces were easily removed with a reducing plasma afterglow at atmospheric pressure, but were harder to remove on silver-copper alloys. In this study we investigated by synchrotron x-ray photoelectron spectroscopy the effect of plasma afterglow on tarnished pure silver, pure copper and sterling silver alloy. The results confirmed that plasma was able to reduce in depth all sulphides except Cu_2S. The process was explained by standard reduction potentials and allowed to draw a detailed picture of the submicrometric evolution of the tarnished layers.

Keywords
heritage; plasma afterglow cleaning; XPS; silver alloys; copper; sulphide

1. Introduction
It is well known that ppb-amounts of H_2S in ambient air are sufficient to cover white and shiny silver alloy objects with a dark film [1]. Jewellery, liturgical attributes or photographic media are all prone to this kind of degradation. Such tarnish films usually result in loss of readability of the objects. To restore the original lustre, often silver dip, electrochemical reduction or polishing techniques are applied on the surface [2,3]. However, for mixed media objects such as silver threads in textile or silver foils on wooden statues, the traditional cleaning methods for silver can hardly be used due to the inevitable chemical damage or mechanical abrasion of the very sensitive organic materials that are in close contact with the tarnished silver. A dry, non-contact cleaning technique such as an afterglow generated by plasma at atmospheric pressure might be a solution for mixed media objects to reduce sulphide compounds [4-6]. The microelectronics field has already studied this topic [7], evaluating the use of the atmospheric pressure He/H_2 plasma for copper oxide reduction. The atomic hydrogen, produced by the discharge, was proposed as the main actor of the process by adsorption and diffusion in the solid. On plasma exposure, the Cu/Cu_2O interface gradually shifts from the surface towards the inner region while the diffusion of hydrogen in the reduced layer was considered as the rate determining step. This hypothesis was supported by the evidence that the quantity of hydrogen atoms transported

towards the solid surface agreed satisfactorily with the quantity consumed in the Cu_2O layer. The process was also confirmed for atmospheric pressure jets where samples are exposed directly to the plasma [8]. However, as a remote plasma configuration is used, where plasma density close to the sample surface is an order of magnitude lower than between the electrodes, the reduction process is still preforming on CuO but dramatically slowed down for Cu_2O [9]. In addition, the reduction process on copper oxide was observed also in absence of hydrogen, suggesting that not only the hydrogen atoms are involved but also plasma electrons [10]. Following this intuition, the combined use of hydrogen and free electrons to trigger electrochemical reactions were tested for surface patterning applications using plasma jet on metal oxides films [11]. Despite these encouraging results in electronics applications, the implementation of the plasma dry cleaning on mixed media objects to reduce sulphide compounds for cultural heritage restoration is scarcely investigated. Moreover, in these cases, the understanding of the mechanism is mixed up by the presence of alloys and of natural corrosion which lead to the coexistence of several sulphides and oxides. Most "silver" objects are actually composed of Ag-Cu alloys where the minor amount of copper plays a dominant role in the corrosion process. Therefore, to evaluate the cleaning performance of an afterglow plasma, it is not sufficient to know what the afterglow is doing only on Ag_2S but also on copper sulphides. For that reason, in a previous investigation [12], we exposed to a dielectric barrier discharge (DBD) plasma jet in remote configuration, using He-H_2 as process gas, the sulphidised surface of (1) pure silver with at least 99.9 w% Ag (Ag999), (2) sterling silver with an amount of 7.5 w% of Cu (Ag925) and (3) pure copper containing at least 99.9 w% Cu (Cu999). The plasma treatment clearly indicated different results on the three investigated substrates:

- **Ag999:** The afterglow was able to reduce sulphide compounds into their metallic form in a matter of a few seconds, but the cleaning efficiency drops for corrosion layers thicker than 220 nm. The result is confirmed also by other authors in literature [13];
- **Ag925:** The corrosion layer of this silver alloy contains both Ag-rich and Cu-rich corrosion products [14]. The afterglow was able to reduce a large fraction of the Ag-rich corrosion products while Cu-rich corrosion products were only partially reduced. Besides the problem of the partially reduced copper sulphides, the surface colour appears sometimes pinkish for unknown reasons;
- **Cu999:** Plasma treatments had almost no visual impact on corroded Cu999. However, we demonstrated that at the sub µm-scale the original corrosion layer was covered with a new but unknown phase consisting of spheroidal nanoparticles [14].

More conventional analytical techniques such as electrochemical techniques or electron microscopy did not result in unambiguous information to understand these surfaces modifications. To improve the understanding of plasma treatments effects, we studied in this paper the transformations of ultimate surface region (nm) induced by the afterglow. The chemical speciation of metallic and artificially sulphidised Ag999, Ag925 and Cu999 was investigated before and after plasma treatment by X-ray photoelectron spectroscopy using the NanoESCA beamline (Electron Spectroscopy for Chemical Analysis at the Nanoscale) at Elettra Sincrotrone Trieste. The results obtained allowed to review the layered structure of the corroded layers at the sub-µm level, highlighting its evolution as a function of the corrosion process and the following plasma cleaning stage. In addition, this improved description of the surface evolution permitted to suggest an extension of the electrochemical metal oxides reduction mechanism introduced in the electronics field [10] to Ag,Cu sulphides. The proposed model highlights the complementary action of hydrogen atoms and electrons for silver sulphide and copper monosulphide reduction and explains the unsuccessful result on Cu_2S. The layered structure of the corroded layers at the sub-µm level are than reviewed, highlighting its evolution as a function of the corrosion process and the following plasma cleaning stage.

2. Experimental

2.1. Sample preparation

Three different metal substrates were considered in metallic and artificially sulphidised state: Ag999, Ag925 and Cu999. For each metal type, (1) the metallic and (2) the sulphidised surface was analysed before and after plasma treatment, leading to 4 samples per metal type. The description of the metals used, the procedure to obtain artificially generated sulphide layers and the treatment of the samples with the reducing plasma afterglow with 5% hydrogen in helium at atmospheric pressure can be found in a previous work [12]. The samples were unavoidable exposed to air between the sample preparation (e.g., plasma treatment) and the XPS measurements. Therefore, the adventitious carbon on the surface, which was probably removed by plasma treatment, could be observed for all the plasma treated surfaces. In order to fit the samples in the sample holder of the XPS instrument, small squared samples of 10 mm × 10 mm were cut from the coupons. This was done with a jeweller's saw, using nitrile gloves and removing saw dust from the surface with purified canned air. The squared samples were taken from the most homogeneous regions of the coupons.

2.2. Reference materials

To facilitate the interpretation of the XPS analyses, a series of reference materials was analysed as well. The metallic surfaces of Ag999, Ag925 and Cu999 were considered as reference for the metals. For the corrosion products, powders of respectively Ag_2S (99.9%), Cu_2S (99.5%) and CuS (99.8%) were purchased at Alfa Aesar and pressed into pellets. About 0.1 g of powder was transformed into a pellet of 8 mm diameter and about 1 mm thickness by means of a hand press using a pressure of 3 to 4.5 ton/cm^2. The pellets had a glossy surface and could easily be transported and be manipulated without physical damage. Before these pellets could be analysed with XPS, outgassing was needed. This was done in the preparation chamber of the XPS-instrument. Except for carbonaceous matter, no systematic surface contamination introduced during the sample preparation could be detected. Moreover, no disturbing surface charging occurred during the analyses of the pellets.

2.3. NanoESCA beamline

The instrument installed as an endstation at the NanoESCA beamline of the Elettra storage ring combines an electrostatic Photo Electron Emission Microscope (PEEM) with a double-hemispherical ('IDEA') analyser, allowing the collection of photoemission electron microscopy (PEEM) images, X-ray photo electron-energy-filtered images and XPS spectra as described in the list below. The used setup is shown in Fig. 1. The NanoESCA beamline provides electromagnetic radiation with variable polarization (linear, circular) and energies up to 1300 eV [15]. For most analyses, no preceding cleaning procedure by applying Ar^+ ion sputtering was needed to remove unwanted top layers. However, to visualize the Cu-inclusions in metallic Ag925 with XPS imaging, the surface needed to be cleaned in the preparation chamber of the XPS instrument (kinetic energy Ar^+ ions 2.0 keV, 13-15 µA on the sample, 10-20 minutes per cycle). For sulphidised Cu999 after plasma treatment, the top layer was removed by 2 subsequent cycles.

- **Threshold PEEM images:** The sample was illuminated with UV-light using a high-pressure mercury arc lamp, while the kinetic energy of the secondary electrons leaving the sample surface was measured. The information depth is determined by the escape length of the secondary electrons, which was about 2 nm. In energy filtered PEEM imaging, an image stack was collected by scanning the kinetic energy of the secondary electrons. The PEEM images visualize chemical contrasts because every material has a different PEEM spectrum and a different onset (i.e., photoemission threshold or work function).

- **XPS energy-filtered image series:** The main application mode of the NanoESCA is the high lateral resolution (c. 50-150 nm) mapping of core-level photoemission signatures. Photoelectron energy-filtered image series was acquired for Cu3p, Cl2p, S2p, C1s, Ag3d using a soft-x-ray source of 450 eV. Images for O1s were collected at 600 eV while images for Cu2p were obtained at 1250 eV. The total energy resolution (analyser + beamline) was 0.2-0.3 eV. First, an energy scan was performed by collecting a series of images with an energy step of 0.1 eV within an energy range where the specific signal was located. From the image with the highest contrast, an average image was determined by collecting several images at the optimal energy.
- **XPS spectra:** The fast overview and high-resolution narrow spectra were collected under the same conditions as described for the energy-filtered image series. Energy calibration was performed by localizing the Fermi level position in the valence band spectra and setting that point to zero. For this, least-squares fitting was applied on the near-rectangular shape in the vicinity of the Fermi level using the CasaXPS software version 2.3.15 (CasaXPS Software Ltd. UK [CasaCookBook; www.casaxps.com]). However, for some surface states the expected near-rectangular shape in the vicinity of the Fermi level was too small for energy calibration. In such cases, the energy calibration was refined by using characteristic features in the shape of the valence band spectra [16]. This was done by comparing the shape of the complete valence band spectrum with valence band spectra of similar shape that could be calibrated with least square fitting. Therefore, the procedure applied considers the energy shifts due to surface charging. In any case for further reliability all the analysis is performed by comparison with reference samples measured and analyzed with the same procedure. A detailed description of this method can be found in the Supplementary Material (SM).

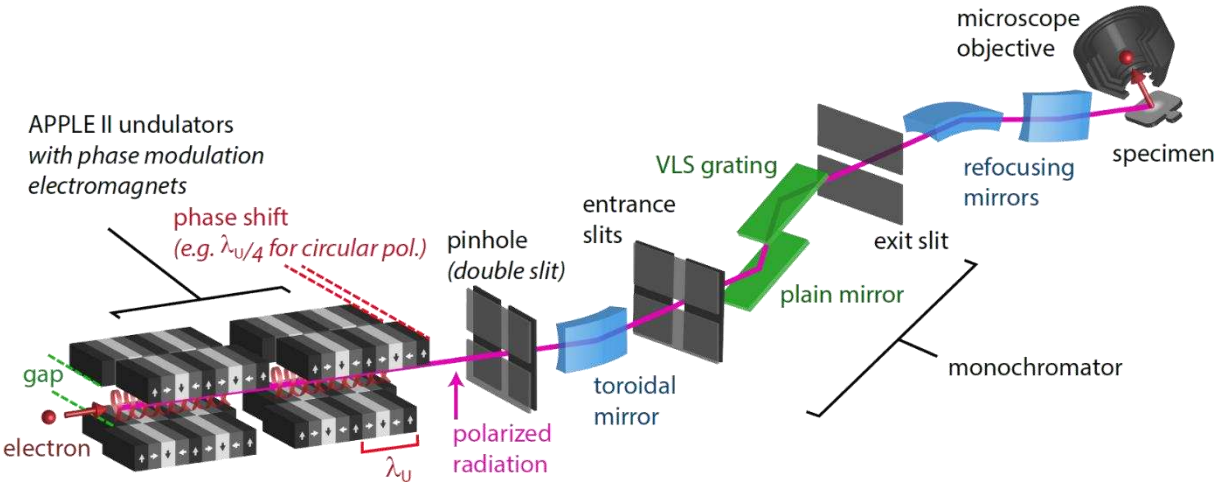

Fig. 1: Scheme of the NanoESCA beamline at Elettra. The gap and the phase shift of the two undulator columns can be adjusted to generate photons with a specific energy and polarization (vertical linear, horizontal linear, left or right circular). Unwanted radiation is stopped by the pinhole and the transmitted beam is demagnified by a toroidal mirror before it enters the monochromator. The angle of the plain mirror and the grating can be adjusted to reflect a nearly monochromatic beam with the desired photon energy onto the exit slit. The width of the exit slit determines the final energy resolution. The refocusing mirrors finally produce a small beam spot on the specimen.

4. Results and Discussion

4.1. Impact of the plasma afterglow on Ag999

The appearance of the samples turned from black to matte silver after the plasma treatment. As already observed in literature [12], on pure silver the plasma action is expected to reduce up to hundreds of nanometres thick layers. PEEM images were taken before and after plasma treatments (Fig. 2). The sulphide surface in Fig. 2a was characterised by an irregular surface. After the afterglow

treatment (Fig. 2b), the rough sulphide film was removed although black spots were still visible in the PEEM image. In previous SEM-EDX observations [12] these spots can be attributed to isolated sulphide particles which can remain on the surface after a plasma treatment. Positioning the beam on such spots no difference in the XPS spectra could be observed. The XPS spectra before and after the treatment are shown in Fig. 3.

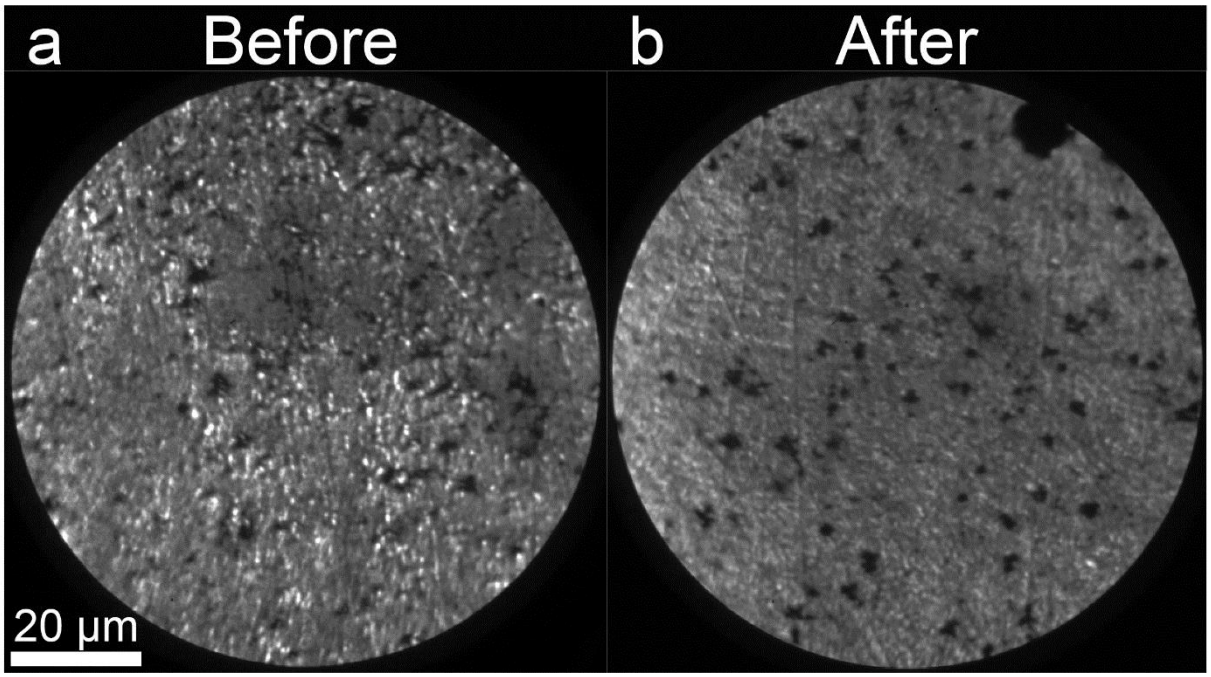

Fig. 2: PEEM images of the sulphide layer on top of Ag999 before and after plasma treatment a) PEEM image of sulphidised Ag999 (E_{kin} = 4.2 eV); b) PEEM image of the same surface after plasma treatment (E_{kin} = 4.5 eV).

A shift of the Ag3d signal towards higher energies could be observed for sulphidised Ag999 after plasma treatment (Fig. 3a). For comparison, the Ag3d spectra of some reference materials were included in Fig. 3a. Before the plasma treatment, the binding energy of the Ag3d peaks corresponds to the Ag_2S reference material, while after the treatment the silver signal overlaps with that of metallic Ag999. The Ag3d peaks related to the Ag_2S reference sample broaden relative to metal peaks, probably due to surface charging since it is a compressed powder pellet. Graedel et al. [1] reported that the Ag3d5/2 signal for Ag, Ag_2S and sulphidised silver ranges between 367.8 eV and 368.0 eV (i.e., a difference of 0.2 eV), while for the silver signal in Fig. 3a, the peak energies ranges between 367.2 eV and 368.0 eV (i.e., a difference of 0.8 eV). This was a substantial larger shift than the reported shifts. In any case, the data within our experimental set-up were self-consistent with our reference samples and supported the reduction of all corrosion products at the surface to metallic silver or at least the surface was covered by metallic silver. In addition, this interpretation was supported by the change of the valance band fingerprint after plasma treatment (Fig. SM-1). On the other side, the S2p signal highlights the presence of polysulphides on sulphidised Ag999 (fig.3b). The polysulphide S-S compounds are characterized by a series of peaks from S^{2-} (160.1 eV – 161.2 eV), S_2^{2-} (162.1 eV- 162.6 eV), S_n^{2-} (161.9 eV – 163.2 eV) to S_n^0 (163.0 eV – 164.2 eV) [17]. No S2p peaks were observed in the energy range 167 eV - 169 eV, meaning that no sulphites or sulphates are present at the surface. After plasma treatment, the surface appeared to consist of Ag_2S with the main S2p peak at 160.6 eV. The results are consistent with literature where the transformation of Ag_2S into metallic silver by means of reductive plasma at low pressure [18-21] or at atmospheric pressure [4] is already reported. The presence of monosulphides as detected by the XPS-analyses after the plasma treatment disagrees with the results obtained on Ag3d signal and by visual inspection since the surface turns from almost black

to dull metal). The explanation may be found in the rough nature of the converted corroded layer and the reactivity of silver to sulphur after exposure to air. Chemisorption and physisorption of a gas on clean metal surface cause only very small shifts and peak broadening of the metal peaks [22-26]. This hypothesis is also supported by the small sulphur signal which can also be detected on polished silver samples after plasma treatment (Fig. SM-2). Therefore, the sulphur signal is probably due to just a surface contamination after plasma treatment and atmosphere exposure.

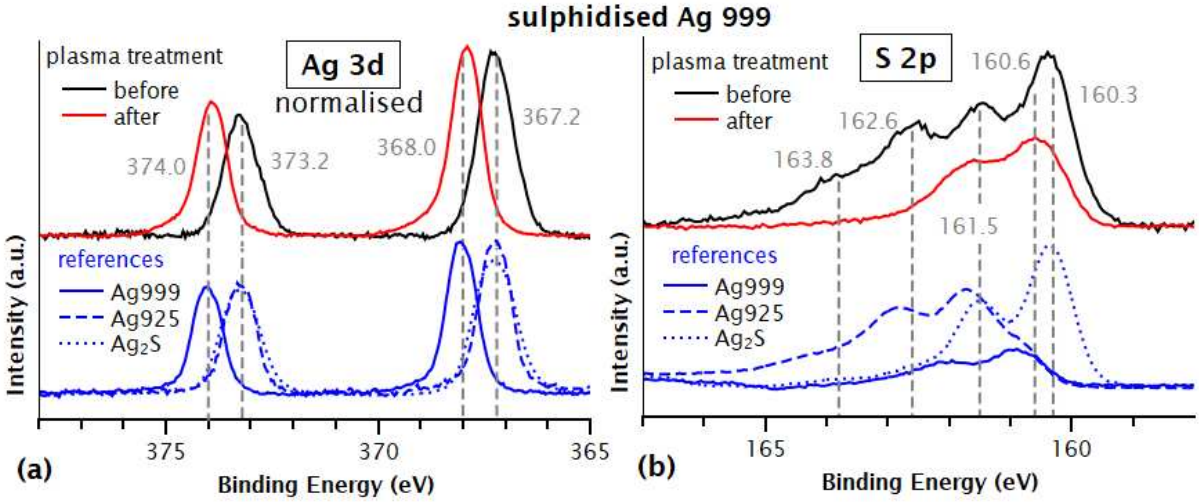

Fig. 3 High resolution spectra of Ag3d (a) and S2p (b) using a soft-x-ray excitation of 450 eV collected of Ag999 from a region of 90 µm diameter of the sulphide layer before (black) and after (red) plasma treatment, compared with reference spectra (blue) of metal (Ag999, Ag925) and Ag_2S powders pressed in pellets. There spectra and peaks within the spectra are normalized to Ag3d5/2.

4.3. Impact of the plasma afterglow on Ag925

It is known that metallic Ag925 consists of an Ag-rich matrix containing small Cu-rich inclusions [27-31]. The PEEM images of metallic, non-sulphidised Ag925 were able to visualize the Cu-rich inclusions in the alloy (images not shown here). XPS-imaging can only visualize these inclusions after the removal of a top layer by Ar ion sputtering from the metal surface. The XPS images of the surface after the ion sputtering are shown in Fig. 4. The brighter zones in Cu3p3/2 image (Fig. 4a) correspond to the darker regions in the Ag3d5/2 image (Fig. 4b). The Cu-rich inclusions had a size of 1 µm – 2 µm. The valence band (Fig. 4c) changed substantially as a consequence of the cleaning procedure: after cleaning the spectrum was similar to that of metallic copper (Fig. SM-4). The Ag3d signals endured a chemical shift of less than 0.2 eV due to the removal of some sulphides (Fig. 4d). Although the cleaning procedure was useful to highlight the copper inclusions in the silver matrix, it was not used on the other Ag925 samples to avoid the distortion of the information about the corrosion layer.

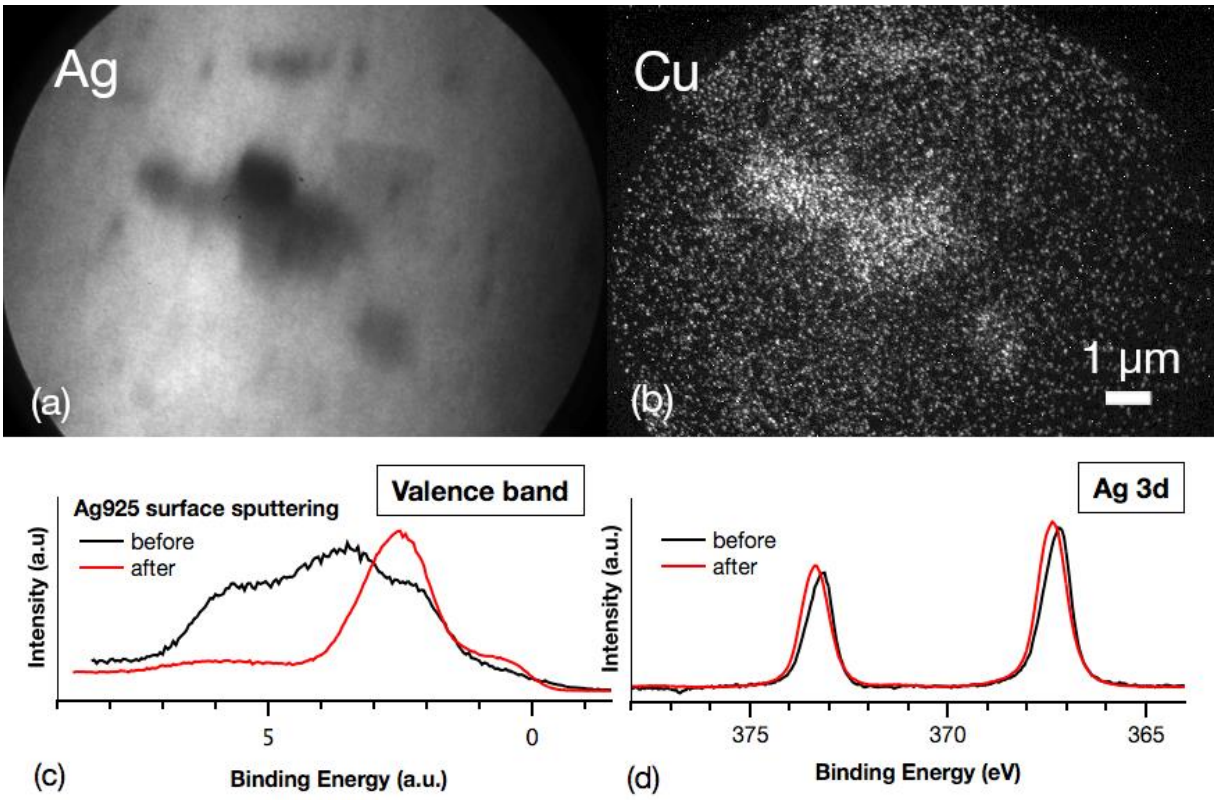

Fig. 4: XPS images collected of metallic Ag925 after cleaning by Ar sputtering for 20 minutes (field of view = 13 µm); a) average of 10 XPS images collected for Cu3p3/2 (x-ray excitation = 450 eV; Ekin = 374.3 eV); b) Average of 10 XPS images collected for Ag3d5/2 (x-ray excitation = 450 eV; E_{kin} emitted electrons = 81.0 eV); c) Valence band spectra before and after the sputtering procedure; d) High-resolution narrow spectra of Ag3d collected before and after the sputtering procedure.

For sulphidised Ag925 before plasma treatment, the PEEM images and SEM-EDX analyses were published elsewhere [14]. That investigation suggested the presence of a heterogeneous microstructure and of a Cu-enrichment at the surface during the corrosion process and the presence of Cu-rich islands in the sulphide layer. The XPS analyses, presented in the same work [14], showed no substantial differences among such islands and an area in-between and suggested that the ultimate surface of the corrosion layer consisted of a thin top layer homogeneous and rich in Ag and in S but poor in Cu. Here we present in Fig. 5 the plasma treatment of sulphidised Ag925. The plasma action led to a shift for the Ag3d5/2 signal from 367.2 eV (i.e., this is close to Ag_2S) to 367.6 eV (i.e., this is between Ag999 and Ag925). The shift to higher energies, even if Ag999 position was not reached, suggests a certain reduction of the sulphidised surface layer. In addition, the high-resolution spectra, as normalised to Ag3d5/2 peak, demonstrated that the monosulphide signal dropped and that the copper signal rose. This increase suggests the formation of a Cu-enriched metallic Ag-Cu layer, which explains the pinkish colour of the treated sample. This interpretation is supported also by the valence band spectrum after the plasma treatment (Fig. SM-1), which is closer to the metallic copper, than to silver.

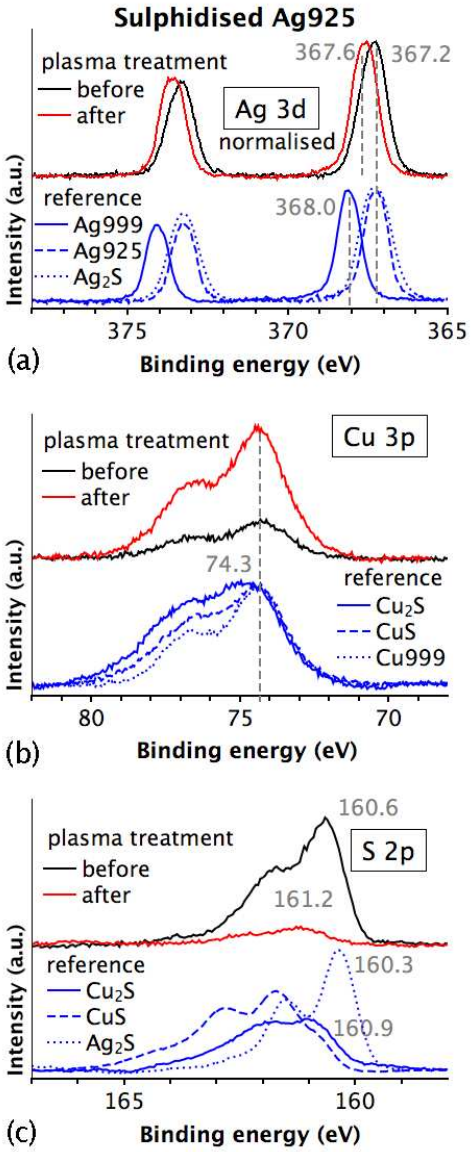

Fig. 5: High resolution spectra of Ag3d, Cu3p and S2p using a soft-x-ray excitation of 450 eV. Spectra are normalised to Ag 3d5/2. Spectra were collected from sulphidised Ag925 before (black) and after (red) plasma treatment. XPS spectra are compared with reference spectra (blue).

4.4. Impact of the plasma afterglow on Cu999

In Fig. 6 are presented the XPS spectra of the tarnished Cu999 sample, before and after the plasma treatment. The corroded surface, as is, was characterized mainly by Cu_2S, the fingerprint signal of the sulphide is clearly visible on the S2p spectrum, when directly compared to the reference samples (Fig. 6b). After the plasma treatment the remaining S2p signal is negligible relative to background, highlighting an efficient surface copper reduction. The Cu3p peak showed to be less sensitive to the plasma treatment since the spectra before and after plasma treatment overlap (Fig. 6a). This surface reduction is in contrast with previous analyses, where we showed with micro-analytical techniques that the corrosion layer existed even after the plasma treatment [12].

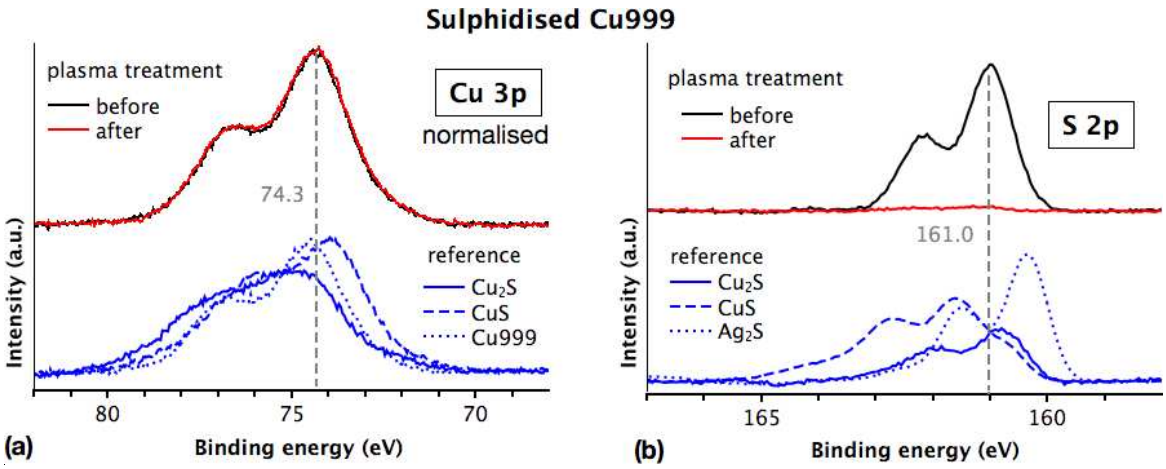

Fig. 6: High resolution spectra of Cu3p and S2p using a soft-x-ray excitation of 450 eV, signals normalised to Cu3p3/2. Spectra were collected of sulphidised Cu999 before (black) and after (red) plasma treatment. High resolution XPS spectra are compared with reference spectra (blue).

To solve this inconsistency, a depth profiling was performed after the plasma treatment with two subsequent sputtering cycles of 10 minutes each. The copper peak did not show any energy shift due to the sputtering process (Fig. 7). The sulphide signal, instead, became visible again after sputtering and increased as the sputtering process proceeded. Therefore, the plasma was able to reduce the Cu_2S at the surface, forming a metallic copper film of few nanometers thick, but the corroded layer still remained untouched underneath. The formation of a such thin metallic Cu film could not change the appearance of the surface, which was left visually matte black. The absence of sulphide on the surface of copper after the cleaning and exposure to air (Fig. SM-4, S2p of the metal surface), reflects the difference in reactivity of the two metals relative to the exposure to air after the plasma treatment.

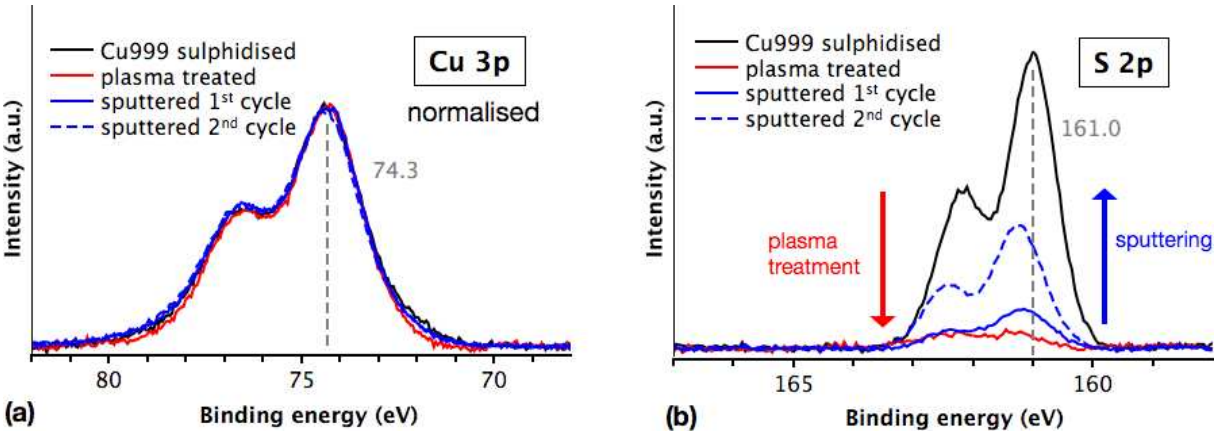

Fig. 7: High resolution XPS spectra collected of sulphidised Cu999 metal before and after H_2/He plasma treatment and then after two subsequent sputtering cycles. The red arrow in (a) highlights the decrease of the sulphur signal after the plasma treatment, while the blue arrow shows its increase due to the following sputtering cycles.

4.5. Samples surface evolution

The analyses presented demonstrated that the first nm of the corrosion layer is different from the rest of that corrosion layer. That top layer endured drastic changes during the treatment with the afterglow. In Fig. 8, the evolution of the corroded layer in the different samples is visualized from its formation to its state after the plasma treatment. That mechanism is mainly based on previously published results [12,14], but the information supplied by the XPS investigation in this study allowed to highlight the chemical composition of the ultimate topmost layer.

Ag999

The corrosion layer is formed after metallic Ag999 immersion in a Na_2S solution. This resulted in a submicrometer thick and rough corrosion layer, composed at the surface of polysulphide species. After plasma treatment, the sulphide layer was effectively reduced. The reduction affected the whole layer thickness [12,14], except for some remnants of larger sulphide particles. In this work, the XPS analyses highlighted the full shift of silver to the metallic state, the vanishing of the polysulphides, and the appearance of monosulphides probably due to air exposure. These observations suggest that on the surface of plasma treated Ag999 there is a metallic silver layer on the whole sample surface, even on those micrometric sulphide particles.

Ag925

The sulphidised Ag925 surface contains mainly Ag_2S and lower contribution of CuS and Cu_2S (Fig. 5). Few nanometres below that top layer, the corrosion layer showed a heterogeneous structure containing islands of Cu-rich corrosion products due to copper migration to the surface [12]. After the plasma treatment, a drastic drop of the sulphur signal and a rise of the copper signal were recorded. This increase in copper content is coherent with the migration of copper to the surface during the corrosion layer formation, which led also to a pinkish colour of the sample. Therefore, as previously observed [12], the dendrites on top of Cu,S-rich islands disappeared, but Cu^+ rich islands still remain below. It should be noted that the pinkish colour was not observed for all cases. It is known that copper in Ag925 corrodes preferentially and that silver corrodes in a later stage [14]. Therefore, a more severe corrosion result in more Ag_2S on the surface and after reduction a thicker and rougher grey silver layer can be formed.

Cu999

The corroded layer is mainly composed by Cu_2S. The surface treatment led to the formation at the sub µm-level of a surface nanostructure detected by SEM-EDX [12]. This result agrees with the formation of the few nanometers thick metallic Cu film after the plasma treatment as observed by XPS. The reduction is limited to the ultimate top surface, the corroded layer remains unaltered underneath.

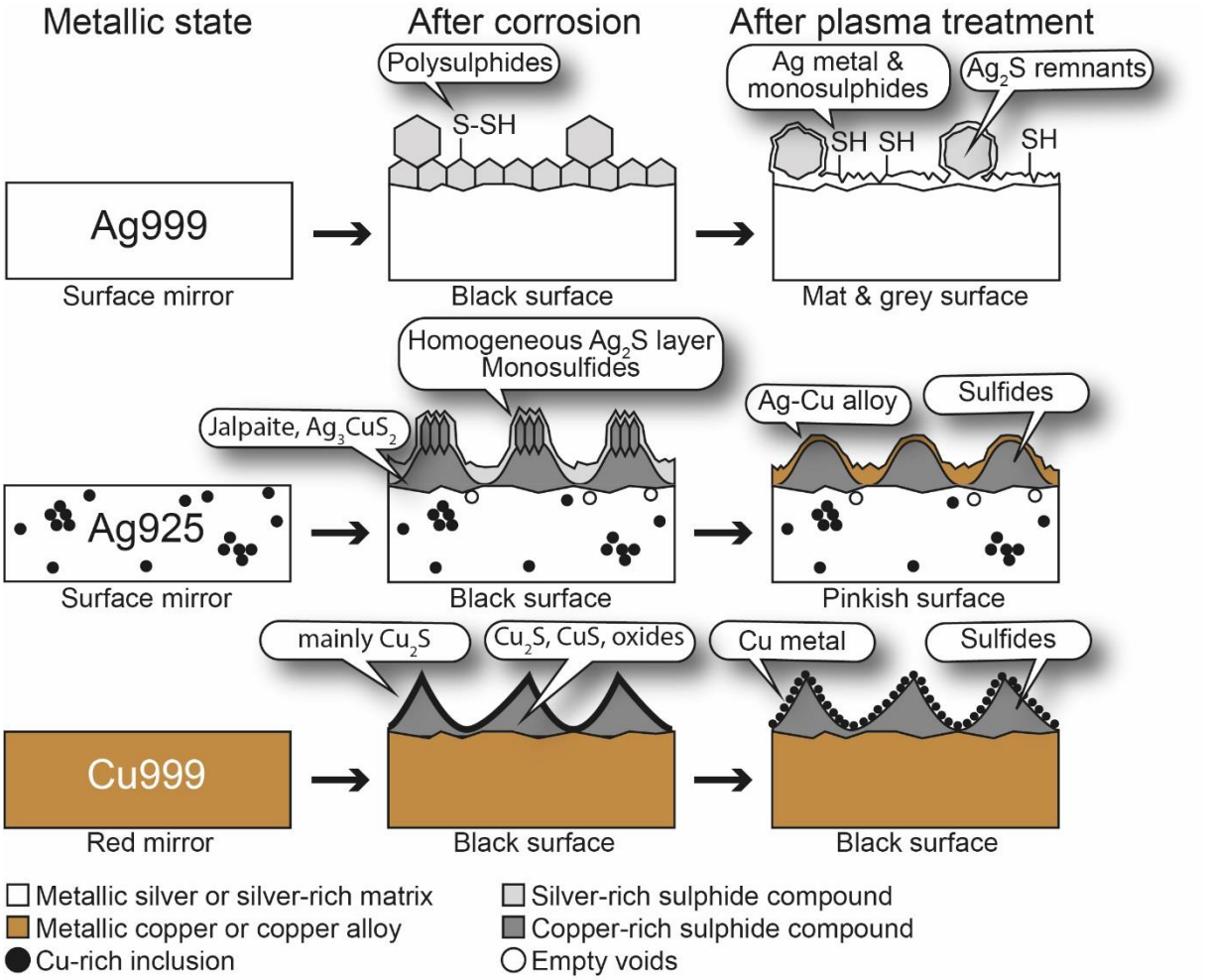

Fig. 8: Evolution of Ag999, Ag925 and Cu999 sample as a result of corrosion and plasma afterglow treatment visualized in cross-section.

4.6. **Model of the reduction mechanism**

The presented XPS analyses showed that the submicrometric corroded layer of Ag_2S on pure silver can be fully reduced as suggested also by literature in all its thickness, except for some larger Ag_2S remnant particles. On the other side, sterling silver (Ag925) showed a general reduction of the surface resulting in a copper enrichment, but at the same time the abundant amounts of Cu_2S remained underneath. Lastly, the afterglow treatment led to the reduction also of the sulphidised pure copper, but this is limited to its ultimate surface directly exposed to the afterglow. Therefore a few nanometers thick metallic copper layer is formed on the top of the tarnishing.

As for the copper oxide [7], the results obtained can be interpreted considering an electrochemical reduction mechanism. The plasma environment at atmospheric pressure and room temperature is, indeed, characterized by a high density of ions and electrons (n = 10^{10}-10^{14} cm^{-3}), meta stable species, radicals and photons [32]. The values of the different parameters can change as a function of the configuration. Plasma can supply the right ingredients to induce non-thermal electrochemical reaction in the gas/solid phase. The electrochemical reduction of Cu_2O by atmospheric pressure plasma jets has been already shown even in absence of hydrogen [10]. In this condition, the reduction reactions which can occur in our experiment can be summarised as

$Ag_2S + 2e \rightleftharpoons 2Ag + S^{2-}$ $\quad E_0$ = -0.691 V

$CuS + 2e \rightleftharpoons Cu + S^{2-}$ $\quad E_0$ = -0.730 V

$Cu_2S + 2e \rightleftharpoons 2Cu + S^{2-}$ E_0 = -0.900 V

, where E_0 is the standard reduction potential [33,34]. It can be concluded that in absence of hydrogen molecules, the reactions will not occur spontaneously. In our experiment, we worked with a He/H_2 process gas. Therefore, we can assume the presence of hydrogen atoms, protons and free electrons at low temperature. The afterglow configuration, indeed, does not hinder the reactive species to reach the sample surface, even if in lower concentration than in the bulk of the plasma [35-37]. The standard reduction potentials drastically change with the supply of hydrogen ions. The electrochemical reactions then become

$Ag_2S + 2H^+ + 2e \rightleftharpoons 2Ag + H_2S$ E_0 = -0.0366 V
$CuS + 2H^+ + 2e \rightleftharpoons Cu + H_2S$ E_0 = +0.100 V
$Cu_2S + 2H^+ + 2e \rightleftharpoons 2Cu + H_2S$ E_0 = -0.270 V

In this case, the CuS and Ag_2S reduction is close to 0 V and with a minimum of extra energy these reduction reactions will occur spontaneously. The results, indeed, demonstrated that a rather thick layer of Ag_2S could be reduced, and the presence of H_2S in the exhaust of the reactor is confirmed in literature [5]. The removal of H_2S makes the reduction process irreversible. In addition, since the reduction process is not limited to the topmost exposed layer, the electrons and hydrogen atoms are expected to migrate through the surface, as already speculated for copper oxides [7]. The migration of atomic hydrogen in polycrystalline structures, indeed, have been already observed and demonstrated a high mobility [38]. This means that some semiconductors will endure a spontaneous reduction process in contact with the afterglow while other will not endure such an electrochemical reaction.

The Cu_2S needs the supply of extra energy (i.e., temperature) or a shift in the chemical equilibrium as described by the Nernst law in aqueous solutions to make the reaction spontaneous. This result is consistent with literature, where the Cu_2O becomes not efficient as an afterglow configuration is used [9]. With direct plasma exposure, contrary to afterglow configuration where the density of charged species is orders of magnitude lower, not negligible biasing can easily appear on the sample due to surface charging and to its involvement as electrode in the plasma electrical scheme [39]. Therefore, with direct exposure to plasma the extra-energy can be straight supplied by a voltage development. The extra energy to promote the reaction can be in principle supplied also thermally. However, this solution is usually avoided in atmospheric plasma processes which aim to be non-thermal. In our case, in particular, the gas temperature of the afterglow configuration was kept below 40°C to avoid damage on heritage objects. However, our results demonstrated that Cu_2S could be transformed on tarnished Cu999, forming of a few nanometers metallic layer. The reduction is limited to the ultimate surface. Therefore, the spontaneous occurring reduction of Cu_2S cannot be explained by temperature or voltage of the substrate. Therefore, the most probable candidate energy-supply by the afterglow which can cause a spontaneous reduction are hydrogen atoms concentration or photons. At the surface, indeed, a higher H atoms concentration can be found since it is accessible directly by the hydrogen in the afterglow, while in the solid the concentration is mediated by the diffusion process. On the other side, an additional energy support may be offered by plasma Vis-UV emissions, which are absorbed in the first nanometers of the sample and generates electron-hole pairs in the semiconductor [40], considering that Cu_2S has been also regarded as a promising solar energy conversion material [41].

The proposed model well agrees also with the reduction exceptions of the Ag999 and Ag925 samples. On Ag999, after the plasma treatment still remains some dark spots in PEEM which correspond to Ag_2S

microparticles covered by a reduced silver shell. Such metal layer may form a conductive shell, which may hinder the electrochemical reduction of the inner core of the particle. On the other side, on Ag925 after the plasma treatment still remain some Cu_2S inclusion in a reduced matrix. This effect is consistent with the electrochemical interpretation of the process where the Cu_2S is harder to reduce than CuS and Ag_2S, without an additional energy support or equilibrium shift.

5. Conclusions

The XPS investigation of corroded samples (Ag999, Ag925 and Cu999) before and after a plasma afterglow treatment with a reducing atmosphere (He/H_2) demonstrated that the results were highly affected by the alloy composition and the chemical compounds present in the corrosion layer.

In all the samples Ag999, Ag925 and Cu999, always, the plasma treatment led to a reduction process and the formation of a metallic film over the whole surface. In addition, we highlighted that Ag_2S and CuS could easily be reduced even in a certain thickness, while Cu_2S reduction was limited to the first few nanometers only. However, in all samples some sulphides remained for different reasons. In Ag999 the microparticles of Ag_2S could not be reduced in their inner core and in Ag925 and Cu999 the compounds related to Cu_2S remain underneath the reduced surface. These experimental evidences could be explained by the suggested electrochemical model of the afterglow reduction where the difference in standard reduction potential plays a key role in the process promotion. CuS and Ag_2S present respectively positive and close to zero standard reduction potential in presence of atomic hydrogen, free protons and free electrons. On the other side, Cu_2S reduction could only be promoted by changing the reaction conditions. In our experiment this change may be due to a higher hydrogen atom concentration or to photons. However, following the model proposed, alternatives can be found in sample heating or in direct exposure to plasma.

From the cultural heritage point of view, the plasma treatment of tarnished “silver” objects appeared to be limited by two phenomena. The first phenomenon was that the copper in silver alloys corrodes preferentially and that the corrosion layer was enriched in copper. When the corrosion layer was reduced back to its metallic state, a pinkish Ag-Cu alloy was formed. This change in colour is not desired in heritage. Also, the typical high gloss of silver objects is lost because the treatment is not able to diminish the surface roughness caused by the corrosion process. The other limiting phenomenon was the conversion of the corroded layers. Contrary to popular beliefs, the corrosion layers on top of Ag-Cu alloys consist of complex mixtures. This makes the result of the plasma treatments difficult to predict. Even if the addition on extra energy may allow to overcome the barrier for the Cu_2S reduction, the problem of an undesired surface appearance due to the copper enrichment exists. This means that the application of a reducing afterglow plasma at atmospheric pressure at this stage, if a full reduction is required, is limited to heritage objects that contain pure silver at the surface and at early corrosion stages.

Acknowledgements

This work was supported by the EU-FP7 grant PANNA no. 282998. The SR-XPS measurements at the NanoESCA beamline of the Elettra storage ring were performed under the approval of the advisory Committee (Proposal No. 20135164).

References

[1] Graedel T.E., Franey J.P., Gualtieri G.J., Kammlott G.W., Malm D.L., On the mechanism of silver and copper sulfidation by atmospheric H2S and OCS, Corrosion Science, 1985, 25(12), 1163-1180

[2] Costa V., The deterioration of silver alloys and some aspects of their conservation, Reviews in Conservation, 2001, 2, 19-35

[3] Degrigny C., Jeanneret R., Witschard D., Local cleaning with the pleco electrolytic pencil of the tarnished saint candide reliquary head at the treasury of Saint-Maurice abbey, Valais (Switzerland), e-PS, 2015, 12, 20-27

[4] Patelli A., Favaro M., Simon S., Storme P., Scopece P., Kamenova V., Kamenarov Z., Lorenzon A., De Voeght F.- EU-Project PANNA: Plasma and nano for new age soft conservation: development of a full-life protocol for the conservation of cultural heritage, Lecture notes in computer science, 2012, 7617, 793-800

[5] Goossens O., Dekempeneer E., Vangeneugden D., Van de Leest R., Leys C., Application of atmospheric pressure dielectric barrier discharges in deposition, cleaning and activation, Surface and Coatings Technology, 2001, 142-144, 474-481

[6] Grieten, E., Schalm O., Tack P., Bauters S., Storme P., Gauquelin N., Caen J., Patelli A., Vincze L., Schryvers D., Reclaiming the image of daguerreotypes: characterization of the corroded surface before and after atmospheric plasma treatment, Journal of cultural Heritage, 2017, 28, 56-64

[7] Sawada Y., Taguchi N., Tachibana K., Reduction of Copper Oxide Thin Films with Hydrogen Plasma Generated by a Dielectric-Barrier Glow Discharge, Japanese Journal of Applied Physics, 1999, 38, Part 1, No. 11, 6506—6511

[8] Tajima S., Tsuchiya S., Matsumori M., Nakatsuka S., Ichiki T., High-rate reduction of copper oxide using atmospheric-pressure inductively coupled plasma microjets, Thin Solid Films, 2011 519(20), 6773–6777

[9] Inui H., Takeda K., Kondo H., Ishikawa K., Sekine M., Kano H., Yoshida N., Hori M., Measurement of Hydrogen Radical Density and Its Impact on Reduction of Copper Oxide in Atmospheric-Pressure Remote Plasma Using H_2 and Ar Mixture Gases, Applied Physics Express, 2010, 3(12), 126101

[10] Sener M.E., Caruana D.J., Modulation of copper(I) oxide reduction/oxidation in atmospheric pressure plasma jet, Electrochemistry Communications, 2018, 95, 38-42

[11] Sener M.E., Sathasivam S., Palgrave R., Quesada Cabrera R., Caruana D.J., Patterning of metal oxide thin films using a H_2/He atmospheric pressure plasma jet, Green Chemistry, 2020, 22, 1406-1413

[12] Schalm O., Storme P., Gambirasi A., Favaro M., Patelli A., How effective were reducing plasma afterglows at atmospheric pressure in removing sulphide layers: application on tarnished silver, sterling silver and copper, Surface and Interface Analysis, 2018, 50(1), 32-42

[13] M. Boselli, C. Chiavari, Vi. Colombo, M. Gherardi, C. Martini, F. Rotundo, “Atmospheric pressure non-equilibrium plasma cleaning of 19th century daguerreotypes” Plasma Process. Polym. 14(3). 2017; e1600027

[14] Schalm O., Crabbé A., Storme P., Wiesinger R., Gambirasi A., Grieten E., Tack P., Bauters S., Kleber Ch., Favaro M., Schryvers D., Vincze L., Terryn H., Patelli A., The corrosion process of sterling silver exposed to a Na2S solution: monitoring and characterizing the complex surface evolution using a multi-analytical approach, Applied Physics A, 2016, 122(10):903, doi:10.1007/s00339-016-0436-6

[15] Schneider C.M., Wiemann C., Patt M., Feyer V., Plucinski L., Krug I.P., Escher M., Weber N., Merkel M., Renault O., Barrett N., Expanding the view into complex material systems: From micro-ARPES to nanocale HAXPES, Journal of Electron Spectroscopy and Related Phenomena, 2012, 185, 330-339

[16] Miller A.C., Powell C.J., Gelius U., Anderson C.R., Energy calibration of x-ray photoelectron spectrometers. Part III: location of the zero point on the binding-energy scale, Surface and Interface Analysis, 1998, 26, 606-614

[17] Smart R., Skinner, W. Gerson A., XPS of Sulphide Mineral Surfaces: Metal-deficient, Polysulphides, Defects and Elemental Sulphur, Surface and Interface Analysis, 1999, 28, 101-105

[18] Daniels V.D., Holland L., Pascoe M.W., Gas plasma reactions for the conservation of antiquities, Studies in Conservation, 1979, 24(2), 85-92

[19] Holland L., Samuel G., The reduction of Ag_2S and treatment of paper in a magnetron glow discharge, Studies in Conservation, 1981, 14, 205-218A

[20] Daniels V., Plasma reduction of silver tarnish on Daguerreotypes, Studies in Conservation, 1981, 26(2), 45-49

[21] Schmidt-Ott, K., Plasma-Reduction: Its Potential for Use in the Conservation of Metals, in Proceedings of Metal 2004, Canberra, National Museum of Australia, 2004, p.235-246

[22] Fuggle J.C., Menzel D., The effect of chemisorption on substrate core levels observed by XPS, Chemical Physics Letters, 1975, 33(1), 37-40

[23] Barrie A., Bradshaw A.M., XPS shifts of substrate core levels upon chemisorption, Physics Letters, 1975, 55A(5), 306-308

[24] Buckley A.N., Woods A., Identifying chemisorption in the interaction of thiol collectors with sulphide minerals by XPS: adsorption of xanthate on silver and silver sulphide, Colloids and Surfaces A: Physicochemical and Engineering Aspects, 1995, 104, 295-305

[25] Ohgi T., Fujita D., Deng W., Dong Z.-C., Nejoh H., Scanning tunnelling microscopy and x-ray photoelectron spectroscopy of silver deposited octanethiol self-assembled monolayers, Surface Science, 2001, 493, 453-459

[26] Lee J.I., Howard S.M., Kellar J.J., Cross W., Han K.N., Electrochemical Interaction between Silver and Sulfur in Sodium Sulfide Solutions, Metallurgical and Materials Transactions B, 2001, 32B, 895-901

[27] Scott D.A., Metallography and microstructure of ancient and historic metals, The J. Paul Getty Trust, 1991

[28] Linke R., Schreiner M., Energy Dispersive X-Ray Fluorescence Analysis and X-Ray Microanalysis of Medieval Silver Coins: An Analytical Approach for Non-Destructive Investigation of Corroded Metallic Artifacts, Microchimica Acta, 2000, 133, 165-170

[29] Beck L., Bosonnet S., Réveillon S., Eliot D., Pilon F., Silver surface enrichment of silver-copper alloys: A limitation for the analysis of ancient silver coins by surface techniques, Nuclear Instruments and Methods in Physics Research Section B Beam Interactions with Materials and Atoms 226(1-2), 153-162

[30] Northover S.M., Northover J.P., Microstructures of ancient and modern cast silver–copper alloys, Materials Characterization, 2014, **90**, 173-184

[31] Van Langh R., Ankersmit H.A., Joosten I., The delamination of silver sulphide layers, in Proceedings of Metal 2004, Canberra, Australia, 4–8 October 2004, p. 137-141

[32] Winter J., Brandenburg R., Weltmann K.-D., Atmospheric pressure plasma jets: an overview of devices and new directions, Plasma Sources Sci. Technol., 2015, 24, 064001

[33] "Electrochemical Series" and "Standard Thermodynamic Properties of Chemical Substances", in CRC Handbook of Chemistry and Physics, 86th ed., David R. Lide, ed., Taylor and Francis, Boca Raton, FL, 2006.

[34] Agocs M., Investigation on the electrode potential of sulfide ores, Acta Mineralogica Petrographica, 1968, 18(2), 61-72

[35] Murakami T., Niemi K., Gans T., O'Connell D., Graham W.G., Afterglow chemistry of atmospheric-pressure helium–oxygen plasmas with humid air impurity, Plasma Sources Science and Technology, 2014, 23, 025005

[36] Murakami T, Niemi K, Gans T, O'Connell D and Graham W G, Plasma Sources Sci. Technol. 23 (2014) 025005 doi:10.1088/0963-0252/23/2/025005

[37] Yue Y., Kondeti V.S.S.K., Bruggeman P.J., Absolute atomic hydrogen density measurements in an atmospheric pressure plasma jet: generation, transport and recombination from the active discharge region to the effluent, Plasma Sources Science and Technology, 2020, 29(4), 04LT01 (5pp)

[38] You S., Patelli A., Ghamgosar P., Cesca T., Enrichi F., Mattei G., Vomiero A., Tuning ZnO nanorods photoluminescence through atmospheric plasma treatments, APL Materials 2019, 7, 081111

[39] Chng T.L., Brisset A., Jeanney P., Starikovskaia S.M., Adamovich I.V. and Tardiveau P., Electric field evolution in a diffuse ionization wave nanosecond pulse discharge in atmospheric pressure air, Plasma Sources Sci. Technol., 2019, **28** 09LT02

[40] L. D. Partain, P. S. Mcleod, J. A. Duisman, T. M. Peterson, D. E. Sawyer, C. S. Dean, L. D. Partain, P. S. Mcleod, J. A. Duisman, T. M. Peterson, D. E. Sawyer, and C. S. Dean, "Degradation of a CuxS / CdS solar cell in hot , moist air and recovery in hydrogen and air," J. Appl. Phys., vol. 54, pp. 6707–6720, 1983.

[41] Yu Y.-X., Pan L., Son M.-K., Mayer M. T., Zhang W.-D., Hagfeldt A., Luo J., and Gratzel M., Solution-Processed Cu2S Photocathodes for Photoelectrochemical Water Splitting , ACS Energy Lett. 2018, 3, 4, 760–766, https://doi.org/10.1021/acsenergylett.7b01326